JOURNAL OF SPACECRAFT AND ROCKETS
Vol. 36, No. 5, September–October 1999

Power Law Shapes for Leading-Edge Blunting with Minimal Shock Standoff

Timothy F. O'Brien* and Mark J. Lewis†
University of Maryland, College Park, Maryland 20742

The application of power law shapes to the blunting of sharp leading-edged vehicles is investigated. Newtonian results have shown that power law shapes exhibit aerodynamic properties similar to geometrically sharp shapes, and power law shapes are close to minimum drag forms for axisymmetric bodies. Power law shapes have, for certain power law exponents, zero radius of curvature (a property of geometrically sharp objects) and infinite slope (a property of geometrically blunt objects) at the nose. These qualities have seemed promising for the design of blunted leading edges with minimum shock detachment distance (and, hence, low drag), which might also have acceptable heating rates. To investigate this, comparisons based on geometry, equivalent drag, equivalent heating, and equivalent shock detachment distance are made between power law configurations and circular cylinder shapes. Two-dimensional computational and analytical results are provided that question the results of Newtonian analysis for power law leading-edge geometries. The analysis also shows that, despite the seeming advantages of power law geometries, circular cylinders provide smaller shock standoff and drag for equivalent stagnation point heating under the range of conditions investigated.

Nomenclature

A = power law constant for curve fit shock wave
B = power law constant for body
C_d = drag coefficient
C_p = pressure coefficient
D' = drag per unit span
h = enthalpy
K = stagnation point velocity gradient, s^{-1}
M = Mach number
n = power law exponent of shock wave
Pr = Prandtl number
p = pressure
Q = heating rate
q = power law exponent of the body
R = radius, cm
s = arc length, m
u = velocity, m/s
V = volume
x, y = dimensions in Cartesian coordinates
δ = shock detachment distance, m
θ = body slope or deflection angle
μ = coefficient of viscosity
ρ = density
ϕ = $\pi/2$ minus body slope angle

Subscripts

cc = circular cylinder
d = drag
e = boundary-layer edge conditions
eq = equivalent circular cylinder
g = generating radius
h = heating rate
pwr = power law
sd = shock detachment distance
w = wall conditions
0 = stagnation point conditions
$\frac{1}{2}$ = conditions for one-half power law geometry
∞ = freestream condtions

Received 19 August 1998; revision received 11 January 1999; accepted for publication 13 January 1999.

*Graduate Research Assistant, Department of Aerospace Engineering; genghis@eng.umd.edu. Student Member AIAA.

†Associate Professor, Department of Aerospace Engineering; lewis@eng.umd.edu. Associate Fellow AIAA.

Introduction

THE successful design of high-lift, low-drag, hypersonic configurations, such as would be applicable to either a high-Mach-number cruiser or accelerator, will depend on the ability to incorporate relatively sharp leading edges that combine good aerodynamic properties with acceptable heating rates. Certain configurations, such as hypersonic waveriders, are designed analytically with infinitely sharp leading edges for shock wave attachment. For practical applications, these sharp leading edges must then be blunted for heat transfer, manufacturing, and handling concerns, with associated departures from ideal performance. Because leading-edge blunting promotes shock standoff, practical leading edges will have shock detachment, making leading-edge blunting a major concern in the design and prediction of flowfields over hypersonic configurations.

Two approaches to adding bluntness to an anayltically sharp edge have been pursued and are shown schematically in Fig. 1 (adapted from Tincher and Burnett[1]). The first is to numerically eliminate leading-edge material until a desired curvature is achieved. This method has the inherent problem that substantial planform area could be lost before leading-edge thickness is acceptable for thin angles of obliquity. The second approach, utilized by Burnett and Lewis[2] in the design of a waverider model, adds material to the upper surface, thereby preserving the planform area and increasing the volume. In both cases, it has been generally assumed that a round leading edge, with constant radius of curvature near the stagnation point, is the appropriate blunting geometry.[3]

Shock standoff distance on a cylinder scales with the radius of curvature, and so cylindrical bluntness added for heating rate reduction will also tend to displace the shock wave. Displacement of the shock wave is especially undesirable in a waverider geometry because these shapes usually rely on shock wave attachment at the leading edge to achieve their high lift-to-drag ratio at high-lift coefficient. With power law shapes ($y = Bx^q$), it may be possible to introduce geometric bluntness for heating rate reduction with less shock standoff, thus allowing the blunted leading edge to more closely represent the original sharp leading-edge flowfield. The idea that this concept may be plausible is based on the work of Mason and Lee,[4] who have demonstrated the curious result that some geometrically blunt configurations may actually behave as if they are aerodynamically sharp. Power law shapes were shown to have zero radius of curvature at the nose and yet have an infinite body slope for certain values of power law exponent. This suggests that there

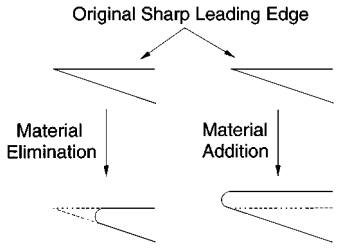

Fig. 1 Leading-edge blunting configurations (adapted from Tincher and Burnett[1]).

may be advantages to using a power law shape as a leading-edge blunting geometry. Zero radius of curvature at the nose will tend to lower shock standoff and drag, whereas infinite slope will tend to decrease the stagnation region heating.

This paper examines the flowfield over power law shapes computationally and compares them to circular cylinder geometries. Comparisons based on geometry, shock detachment distance, drag, and heating are made to examine the benefits and disadvantages of using power law geometries over circular cylinders. Computational solutions and analytical techniques are provided to evaluate these comparisons and determine which geometry is better suited for leading-edge blunting.

Geometric Comparison to Circular Cylinders

There are several comparisons that can be made between a circular cylinder and a power law leading edge. A geometric comparison is first made, to match the process of blunting an analytically sharp leading edge as shown in Fig. 1. The power law shapes are modeled by assuming a sharp leading-edge half-angle θ and then finding a circular cylinder tangent to this wedge with radius R. The circular cylinder radius provides a reference for the amount of blunting desired on the leading edge, for heat transfer and manufacturing considerations. The wedge and the circular cylinder are made to be tangent to a corresponding nondimensional power law body with shape

$$y/R = B(x/R)^q \tag{1}$$

At the matching point of all of these bodies, the body slope angle is equivalent. From these assumptions and a given power law exponent, the power law constant B is

$$B = (\tan\theta/q)^q(1+\tan^2\theta)^{(q-1)/2} \tag{2}$$

The power law shapes analyzed here were assumed to have a leading-edge half-angle of 5 deg, a circular cylinder radius of 2 cm, and a power law exponent of 0.4, 0.5, 0.59, $\frac{2}{3}$, 0.75, and 0.85. Leading-edge dimensions were chosen to be reasonable for a hypersonic cruiser-class aircraft. These shapes are shown in Fig. 2.

One result of this geometric method of comparison is seen in Fig. 2. The volume associated with the power law shapes is greater than that of the comparison circular cylinder for a representative amount of blunting. Hence, for actively cooled leading edges, a larger portion of coolant, endothermic fuel,[5] or catalyst[6] may be placed within the leading edge for heat absorption. It can be shown that the ratio of the volume of a power law body to that of a circular cylinder is

$$\frac{V_{\text{pwr}}}{V_{\text{cc}}} = \frac{2q\cos^3\theta}{(q+1)\sin\theta}\left\{\left[2\tan^{-1}\left(\sqrt{\frac{1-\sin\theta}{1+\sin\theta}}\right) - \sin\theta\cos\theta\right]\right\}^{-1} \tag{3}$$

It is seen from Eq. (3) that the volume advantage of a power law over a cylinder increases as the power law exponent q approaches the wedge value of 1.

Another advantage to power laws may also be seen in Fig. 2. With the additional volume of the power law geometries, these shapes are inherently sharper than the circular cylinder. They are geometrically closer to representing the sharp wedge leading edge than the circular cylinder.

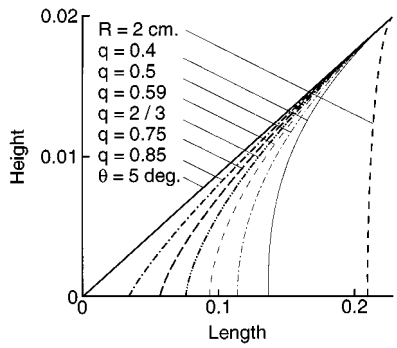

Fig. 2 Power law shapes analyzed and the comparable cylinder, all tangent to a 5-deg wedge (y axis greatly exaggerated).

Computational Solutions

Previous research into power law shapes dealt primarily with axisymmetric configurations, which are especially useful in nose cone and ballistic applications.[7–9] Two-dimensional power law geometries (primarily for leading-edge applications) have primarily been analyzed with approximate methods.[4,8] The most investigated analyses involve Newtonian flow and small disturbance approximations; the former inherently assumes an infinite Mach number, ratio of specific heats equal to 1, and a shock shape that matches the body shape. To obtain a more accurate solution of these flowfields, a computational survey was performed that, in the process, determined the validity of the Newtonian approximations in predicting power law flowfield properties.

The two-dimensional, inviscid, Euler equations were solved for a perfect gas with no chemical reactions on the power law leading edges using GASP 3.0 (Refs. 10 and 11). GASP is a finite volume, conservative, computational fluid dynamics (CFD) code that solves the integral form of the unsteady Reynolds-averaged Navier–Stokes equations in three dimensions. A 190×95 elliptically smoothed grid with orthogonal boundaries at the body surface was used in solving the flow over a family of power law shapes and a circular cylinder shape. The freestream boundary was chosen to ensure shock capture, the symmetry boundary was chosen to maximize the amount of points in the shock layer, and the body surface had grid clustering in the nose region to resolve the stagnation region shock shape and detachment distance. A grid-converged solution was assured by performing a grid sensitivity study on a 190×95, a 95×48, and a 48×24 grid. Results of the sensitivity study showed that the error in both shock detachment distance and drag coefficient was roughly 2% (Ref. 12) between the three solutions using Richardson's extrapolation method.

As a baseline calculation, a CFD solution over a circular cylinder at a Mach number of 6.28 was performed.[11] This Mach number was selected to match the numerical calculations of flowfields over axisymmetric power law bodies performed by Mason and Lee.[4] Shock detachment distance and shock shape had excellent agreement with empirical relations for cylinder-wedges found by Billig.[13] The drag coefficient (referenced to frontal area and neglecting base pressure) was found to be 1.28 compared to the Newtonian solution of $\frac{4}{3}$ and the modified Newtonian solution of 1.24.

A CFD solution for the stagnation region static-to-freestream pressure ratio on a three-quarter power law body is superimposed on the corresponding computational grid in Fig. 3, where the length and height are normalized by the generating circular cylinder radius R. Figure 3 shows that the stagnation region shock is well resolved with the choice of grid point distribution, revealing a discrete, inviscid, shock detachment distance on these shapes, albeit very small. The computational solution for shock detachment distance δ on all of the power law bodies, normalized by R, is shown in Fig. 4. It is seen that for all values of power law exponent, the power law shapes have a shock detachment distance at least 3.5 times smaller than the circular cylinder solution. Furthermore, the inviscid shock detachment distance for the sharpest shape solved ($q = 0.85$) is found to be at least an order of magnitude smaller than the mean free path at sea-level conditions both in front and behind the shock wave. However,

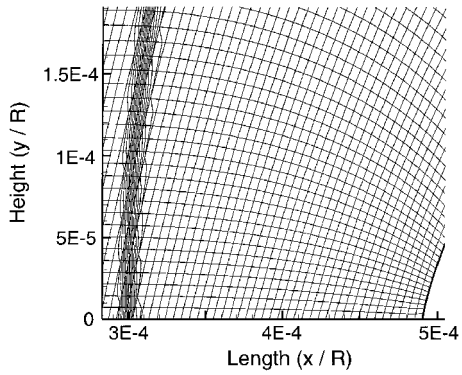

Fig. 3 Normalized static pressure distribution and superimposed grid cells inside shock layer (three-quarter power law).

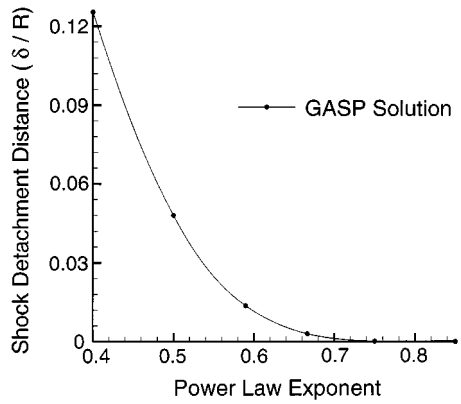

Fig. 4 Computational results for shock detachment distance vs power law exponent.

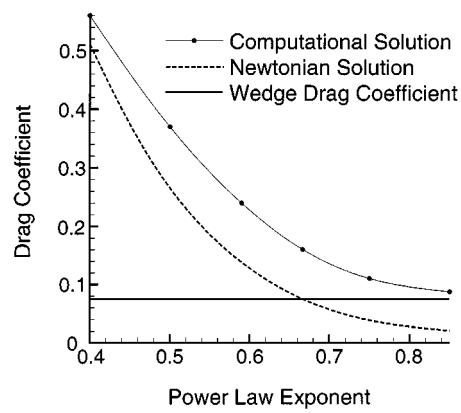

Fig. 5 Drag coefficient vs power law exponent.

viscous effects have been neglected in this analysis, which in reality would increase the shock detachment distance.

The drag coefficient on these shapes (referenced to frontal area and neglecting back pressure) is shown in Fig. 5. It is seen that the computational solution for drag coefficient approaches that of a wedge as power law exponent increases. This trend is expected inasmuch as a wedge is a power law geometry with exponent of 1. Plotted along with the computational solution for drag coefficient is the drag coefficient predicted by Newtonian flow[8]:

$$C_d = \frac{2}{R\cos\theta}\int_0^{R\cos\theta} \frac{(BR^{1-q})^{2/q}q^2y^{(2q-2)/q}}{1+(BR^{1-q})^{2/q}q^2y^{(2q-2)/q}}\,\mathrm{d}y \qquad (4)$$

It is seen from Eq. (4) (plotted in Fig. 5) that Newtonian flow underpredicts the pressure drag coefficient on the power law bodies, which is not surprising because Newtonian theory generally underpredicts the pressure on two-dimensional thin body flowfields.

The pressure gradients in the computational solution can be compared to the predictions of the Newtonian solution provided by

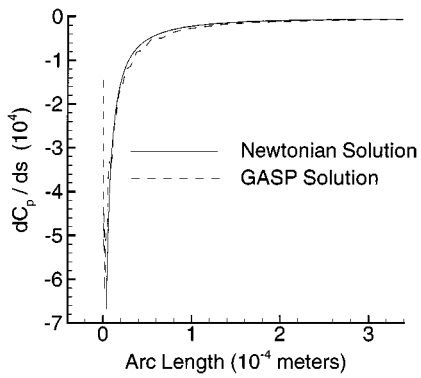

Fig. 6 Gradient in the coefficient of pressure along the arc length for a power law body of $q = \frac{3}{4}$.

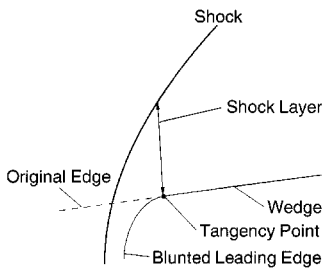

Fig. 7 Location of shock-layer pressure distribution.

Mason and Lee.[4] The gradient of the pressure coefficient along the arc length $\mathrm{d}C_p/\mathrm{d}s$ of the power law bodies defined by Eq. (1) may be found as

$$\frac{\mathrm{d}C_p}{\mathrm{d}s} = -[4(1-q)]\frac{B^2q^2R^{2-2q}x^{2q-3}}{[1+(BqR^{1-q}x^{q-1})^2]^{\frac{5}{2}}} \qquad (5)$$

The Newtonian solution for the gradient of the pressure coefficient in the stagnation region is plotted vs the computational solution for pressure coefficient gradient in Fig. 6 for a power law exponent of $\frac{3}{4}$. The Newtonian solution predicts an infinite gradient in pressure along the arc length as the arc length goes to zero, a result seen for sharp leading edges. However, the computational solution is seen to have a minimum $\mathrm{d}C_p/\mathrm{d}s$ and then returns to zero, a trend seen on blunt leading edges. The CFD solution predicts that the inviscid flows over power law shapes still have a pressure profile comparable to that of a blunt leading edge, despite the radius of curvature at the nose going to zero. This result is expected because it has already been shown that the inviscid shock wave is detached from the leading edge of the power law shapes. Hence, it can be seen that Newtonian theory fails to accurately predict the stagnation region pressure distribution, i.e., drag, on a power law shaped leading edge.

The objective of solving the flowfield over power law leading edges has been to determine whether these shapes can be used to more closely approximate the flowfield over a sharp wedge than a corresponding circular cylinder. Besides shock detachment, leading-edge bluntness (especially on the cowl lip) may also create a significant entropy wake, which could enter an airbreathing engine inlet. In this study, entropy wake effects are quantified by observing the pressure distribution through the inviscid shock layer at the location where the leading-edge blunting merges tangentially with the original wedge geometry (Fig. 7). The static pressure distribution (normalized to the static pressure behind the shock of a 5-deg wedge) is shown in Fig. 8 for the bluntest power law solved ($q = 0.4$), the sharpest power law solved ($q = 0.85$), and the circular cylinder. The cylinder shock layer flowfield is seen to have a significant increase in pressure (nearly a factor of 10) in comparision to the sharp wedge. The bluntest power law investigated ($q = 0.4$) shows a five-fold reduction in overpressure in comparison to the cylinder leading edge and has a more uniform flowfield. For the sharpest power law ($q = 0.85$), a nearly uniform flowfield is found with a pressure increase of 1.3 times the wedge pressure. Hence, if a designer wished to select a blunted leading edge whose flowfield has a more uniform

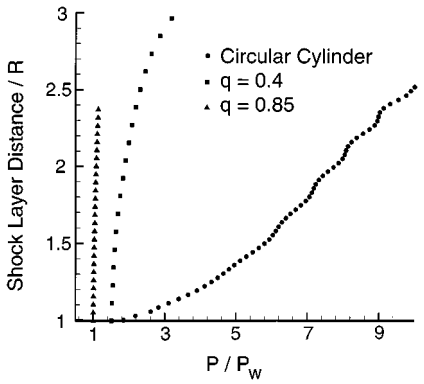

Fig. 8 Normalized pressure distribution across shock layer of various shapes.

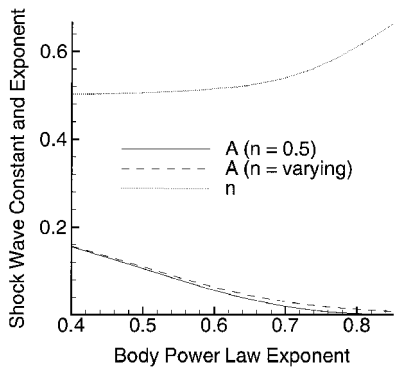

Fig. 9 Shock wave curvefits assuming hyperbolic and varying exponent shock shape.

pressure distribution, a power law geometry could be used instead of a circular cylinder.

Curve fits of the shock shape in the subsonic stagnation region were performed using results from the computational solutions. Shock location was determined by identifying coordinates of the maximum in the second derivative of pressure in the computational solution.[11] The shocks were fitted to power law equations of the form

$$y = Ax^n \tag{6}$$

Two forms of the curve fit were considered in defining the shock shape: 1) assume a hyperbolic shock wave ($n = 0.5$) and find A or 2) vary both n and A. The solutions to these curve fits are shown in Fig. 9. The residual of the curve fits shown was between 99.8 and 99.92%. Both cases exhibit a near linear decrease in A to a power law body exponent of about $\frac{3}{4}$. Furthermore, besides a nearly constant shift, each graph of A follows the same basic shape, suggesting that the assumption of a hyperbolic shock wave shape in the subsonic region of flow is a relatively good approximation regardless of body power law exponent. The shock wave exponent n also displayed a near linear trend to power law exponent of about 0.7. The value for n is seen to be close to hyperbolic, further suggesting again that a hyperbolic shock wave shape is a good approximation in the stagnation region of power law shapes. The curve fits shown in Fig. 9 also demonstrate that the power law exponent of the shock does not equal the power law exponent of the body (zero-order small disturbance prediction[8]). This is also further evidence that Newtonian flow will not accurately predict the stagnation region pressure distribution because the inherent assumption of shock wave shape equal to body shape is not matched.

Stagnation Point Heating Estimation

The stagnation point heating rate is estimated by the classic correlation derived by Fay and Riddell[14] from the stagnation point boundary-layer equations and Sutherland's viscosity relation

$$Q_w = 0.57Pr^{-0.6}\sqrt{\rho_e\mu_e K}(\rho_w\mu_w/\rho_e\mu_e)^{0.1}(h_e - h_w) \tag{7}$$

where Q_w is the stagnation point heating rate, Pr is assumed to be 0.71 in the preceding correlation, and K is the stagnation point velocity gradient (with respect to arc length).

The stagnation point velocity gradient K is found by first assuming Newtonian flow for the pressure distribution.[15] The pressure coefficient C_p may then be found as

$$C_p \equiv \frac{p - p_\infty}{\frac{1}{2}\rho_\infty u_\infty^2} = 2\cos^2\phi \tag{8}$$

Expanding Eq. (8), the derivative of pressure with respect to the arc length at the stagnation point may be estimated as

$$\left.\frac{\mathrm{d}p}{\mathrm{d}s}\right|_0 = -2\rho_\infty u_\infty^2 \phi \frac{\mathrm{d}\phi}{\mathrm{d}s} \tag{9}$$

The stagnation flow region may be considered incompressible because the local Mach number is very small. Using Bernoulli's equation and assuming a linear profile in boundary-layer edge velocity at the stagnation point, the stagnation region boundary-layer edge pressure gradient with respect to arc length may be found:

$$\frac{\mathrm{d}p_e}{\mathrm{d}s} = -\rho_e K^2 s \tag{10}$$

Assuming that pressure remains constant in the normal direction of the boundary layer, the stagnation point velocity gradient assuming Newtonian flow is found by equating Eqs. (9) and (10):

$$K = \sqrt{2\frac{\rho_\infty}{\rho_e}\frac{\phi}{s}\frac{\mathrm{d}\phi}{\mathrm{d}s}}u_\infty \tag{11}$$

where the ratio ρ_e/ρ_∞ is the pitot density ratio. From Eq. (11), the stagnation point velocity gradient on a circular cylinder K_{cc} is estimated by[15]

$$K_{cc} = \sqrt{2(\rho_\infty/\rho_e)}(u_\infty/R) \tag{12}$$

For the power law geometries defined by Eq. (1), the angle ϕ and the arc length s in the limit of small x may be approximated as

$$\phi \approx (1/Bq)(x/R)^{1-q} \tag{13}$$

$$s \approx BqR^{1-q}(q^2 - 3q + 3)x^q \tag{14}$$

From Eqs. (13) and (14), the derivative $\mathrm{d}\phi/\mathrm{d}s$ is

$$\frac{\mathrm{d}\phi}{\mathrm{d}s} = \frac{\mathrm{d}\phi}{\mathrm{d}x}\frac{\mathrm{d}x}{\mathrm{d}s} = \frac{1-q}{q(BqR^{1-q})^2(q^2 - 3q + 3)}x^{1-2q} \tag{15}$$

The stagnation point velocity gradient for the power law geometries using Newtonian flow K_{pwr} is found from substituting Eqs. (13–15) into Eq. (11):

$$K_{pwr} = \sqrt{\frac{\rho_\infty}{\rho_e}\frac{2(1-q)q^{4q}}{q^5(q^2 - 3q + 3)^2}\frac{(\cos\theta)^{2q-2}}{(\tan\theta)^{2q}}}\frac{u_\infty}{R^{2-2q}}x^{1-2q} \tag{16}$$

where θ is the angle of the original sharp leading edge being blunted. Observing Eq. (16), three solutions exist for varying values of body exponent q. For $q < \frac{1}{2}$, the velocity gradient at the stagnation point is zero, for $q > \frac{1}{2}$, the stagnation point velocity gradient is infinite, and for $q = \frac{1}{2}$, a finite velocity gradient $K_{1/2}$ exists:

$$K_{\frac{1}{2}} = 1.61624\sqrt{\frac{\rho_\infty}{\rho_e}}\frac{u_\infty}{R\sin\theta} \tag{17}$$

Assuming that the edge and wall conditions at the stagnation point are identical between a circular cylinder of radius R and a power law shape generated by this cylinder using Eq. (1), for the same Mach number, the ratio of stagnation point heating between the one-half power law shape and the circular cylinder may be found by substituting Eqs. (12) and (17) into Eq. (7):

$$\frac{Q_{w,\frac{1}{2}}}{Q_{w,cc}} = \frac{1.06881}{\sqrt{\sin\theta}} \tag{18}$$

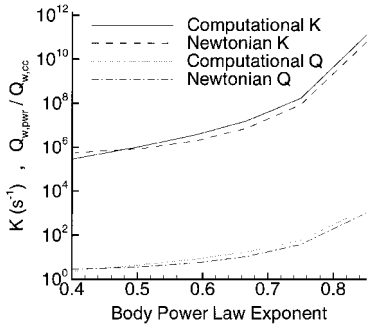

Fig. 10 Stagnation point velocity gradient and heat transfer compared to circular cylinder (Mach 6.28, sea-level conditions).

Equation (18) shows that for all values of sharp leading-edge angle, the one-half power law geometry will always have higher stagnation point heating than a circular cylinder at equivalent stagnation point conditions.

Restating the results, the Newtonian prediction for stagnation point velocity gradient on a power law results in values of zero or infinity for values of $q \neq \frac{1}{2}$. Hence, to compare the rest of the power law geometries with a circular cylinder, the stagnation point velocity gradients were calculated numerically from the computational solution presented earlier. These values are presented in Fig. 10. It was found that the Newtonian solution for K_{cc} and $K_{1/2}$ roughly agreed with the computational results (~20% error).[12] Furthermore, using a characteristic length of the shock detachment distance as a value of x, the Newtonian stagnation point velocity gradient for the rest of the power law geometries is within an order of magnitude of the computational result (Fig. 10). The shock detachment distance was chosen as the characteristic length scale because these geometries have no radius of curvature at the nose.

Using the results shown in Fig. 10, the heating rates on all of the power law geometries may now be compared to the circular cylinder solution. If the edge and wall conditions are assumed the same between the power law geometries and the circular cylinder at the stagnation point, then by inspection of Eq. (7) the ratio of stagnation point heating rates is

$$\frac{Q_{w,\mathrm{pwr}}}{Q_{w,\mathrm{cc}}} = \sqrt{\frac{K_{\mathrm{pwr}}}{K_{\mathrm{cc}}}} \tag{19}$$

where K_{pwr} is the stagnation point velocity gradient on a power law leading edge. The computational and Newtonian results for Eq. (19) are also plotted in Fig. 10. The results compare well, especially for power law exponent between 0.4 and 0.6, giving initial estimates of how power law geometries compare to circular cylinders.

The major result shown in Fig. 10 is that the stagnation point heating is higher on the power law geometries in this geometric comparison than the representative circular cylinder solution. Thus, in general, these shapes behave as if they have a sharper profile than their representative circular cylinder: with smaller shock detachment distance, lower drag, and higher stagnation point heating. However, these shapes have more volume than the circular cylinder geometry. Hence, although stagnation point heating on the power law geometries may be higher, the overall heat transfer to these leading edges may be tolerable if there is active cooling because additional coolant may be placed in the leading edge.

Comparison of Power Law to Circular Cylinder Heating

Certain geometric properties of power law leading edges were compared to a generating circular cylinder. As discussed, one obvious basis of comparison is a geometric one, where leading-edge blunting was done with a power law form that was tangent to the wedge at the same location that the circular cylinder was tangent to the wedge. In Fig. 2 it is noted that the power law geometries have a sharper profile than the generating circular cylinder of radius R, and the power law geometries have more volume than their representative circular cylinder. Hence, it is expected that the shock detachment distance will be smaller for the power law geometries defined. This comparison is not useful in evaluating physical properties, i.e., shock detachment distance, drag, or stagnation point heating. Hence, other bases of comparison will be investigated to further examine the possibilities of using power law shaped leading edges.

Three quantities will be examined: shock detachment distance, drag, and stagnation point heating. Knowing these quantities for the power law geometries, equivalent circular cylinders are found that have the same value of shock detachment distance, drag, or stagnation point heating. These cylinders are then compared to the reference tangent cylinder inasmuch as power law geometries have no characteristic dimension. An equivalent circular cylinder radius for shock detachment distance $R_{\mathrm{eq,sd}}$ may be found by using Billig's correlations on cylinder-wedges[13]:

$$R_{\mathrm{eq,sd}} = 2.591\delta_{\mathrm{pwr}} \exp\left(-4.67 \Big/ M_\infty^2\right) \tag{20}$$

where δ_{pwr} is the shock detachment distance on the power law leading edges (plotted in Fig. 4). Hence, a circular cylinder of radius $R_{\mathrm{eq,sd}}$ will have the same shock detachment distance as a power law with shock detachment distance δ_{pwr}. An equivalent circular cylinder radius for drag $R_{\mathrm{eq},d}$ may be found from

$$R_{\mathrm{eq},d} = R_g \frac{C_{d,\mathrm{pwr}}}{C_{d,\mathrm{cc}}} \tag{21}$$

where R_g is the radius of the circular cylinder used in defining the power law geometries (which was taken as 2 cm) and $C_{d,\mathrm{pwr}}$ is the drag coefficient of the power law geometries (plotted in Fig. 5). Hence, a cylinder of radius $R_{\mathrm{eq},d}$ has the same drag as a power law geometry of drag coefficient $C_{d,\mathrm{pwr}}$. Finally, an equivalent circular cylinder radius for stagnation point heating $R_{\mathrm{eq},h}$ may be found from Eq. (12):

$$R_{\mathrm{eq},h} = \sqrt{2(\rho_\infty/\rho_e)}(u_\infty/K_{\mathrm{pwr}}) \tag{22}$$

where K_{pwr} is plotted in Fig. 10. Equations (20–22) are calculated from the computational results and are shown in Table 1.

Table 1 presents a comparison between the various equivalent radii for power laws of exponent values ranging between 0.4 and 0.85. Taking the $q = 0.4$ values, for example, it is seen that a 0.4 power law shape that is tangent to a 5-deg wedge has the same shock standoff distance as a cylinder that is 3.47 times smaller than a cylinder that is tangent to the wedge at the same point. However, a cylinder with the same drag is only 2.28 times smaller than the reference cylinder, and a cylinder with the same heating rate is 4.45 times smaller. This means that a $q = 0.4$ power law leading edge has 1.28 times the shock standoff distance as a cylinder with the same heating rate. The power law shape also has 1.95 times the drag of the cylinder with the same heating rate. Thus, in matching stagnation point heating performance to a power law geometry, the circular cylinder has smaller shock standoff and lower drag. It appears that the power law geometries are not as promising when detailed heating considerations are involved.

This conclusion is further strengthened by comparing a one-half power law geometry with its original reference cylinder, the equivalent heating circular cylinder, and the circular cylinder with the same radius of curvature at the nose as the power law geometry in Fig. 11 (the one-half power law geometry is the only power law geometry with a definable radius of curvature at the leading edge). It is seen in Fig. 11 that the equivalent heating circular cylinder has a smaller radius of curvature than the one-half power law body. Hence, the equivalent circular cylinder for heating has not only smaller shock

Table 1 Equivalent radii for shock standoff, drag, and stagnation point heating compared to power law generating circular cylinder

q	$R/R_{\mathrm{eq,sd}}$	$R/R_{\mathrm{eq,d}}$	$R/R_{\mathrm{eq},h}$	$\delta_{\mathrm{pwr}}/\delta_{\mathrm{eq},h}$	$D'_{\mathrm{pwr}}/D'_{\mathrm{eq},h}$
0.4	3.47	2.28	4.45	1.28	1.95
0.5	9.43	3.42	16.15	1.79	4.72
0.59	31.85	5.33	58.85	1.84	11.03
0.67	144.24	8.00	251.37	1.72	31.24
0.75	2288	11.57	2766.3	1.25	247
0.85	1.83×10^6	14.68	2.17×10^6	1.19	1.48×10^5

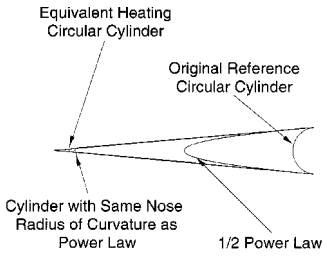

Fig. 11 One-half power law body with original blunting cylinder and equivalent heating cylinder.

detachment distance and drag, but it also has more volume than the power law geometry.

Conclusions

Leading-edge bluntness plays a key role in predicting aerodynamic performance and combustor inlet properties for hypersonic vehicle designs. These aircraft usually rely on sharp leading edges to minimize shock standoff and its associated drag. However, for a leading edge to be practical, some form of blunting must be applied for heating, manufacturing, and handling concerns. Hence, a practical leading edge (usually taken as being a circular cylinder) will tend to displace the shock wave, degrading the predicted performance of originally sharp-leading-edged vehicles.

Power law geometries have been shown to have zero radius of curvature with infinite body slope at the nose. Thus, these geometries have numerical characteristics that could be useful in leading-edge design. From computational and analytical formulations, power law geometries were compared using geometry, shock detachment distance, drag, and stagnation point heating. Results showed that for the same stagnation point heating, circular cylinders have smaller shock standoff and lower drag. Hence, it is concluded that, although power law geometries have numerical characteristics that could be useful in leading-edge design, they cannot be shown to be demonstrably superior to circular cylinder geometries when heating and drag are primary issues.

Acknowledgments

This research was supported by the Center for Hypersonics Education and Research at the University of Maryland (NASA Grant NAGw 11796). The Technical Monitor for this research was Isaiah Blankson of NASA, whose support is greatly appreciated. Computing facilities were provided by James Randolph of the Jet Propulsion Laboratory. Thanks also go to Ashish Nedungadi and Naruhisa Takashima for their efforts and advice in support of the computational results presented.

References

[1]Tincher, D., and Burnett, D., "A Hypersonic Waverider Flight Test Vehicle: The Logical Next Step," AIAA Paper 92-0308, Jan. 1992.

[2]Burnett, D., and Lewis, M. J., "A Reevaluation of the Waverider Design Process," AIAA Paper 93-0404, Jan. 1993.

[3]Kothari, A. P., and Bowcutt, K. G., "Leading Edge Optimization for Hypersonic Vehicles," *Proceedings of the 1st International Hypersonic Waverider Symposium*, Vol. 1, edited by J. D. Anderson, Univ. of Maryland, College Park, MD, 1990.

[4]Mason, W. H., and Lee, J., "Aerodynamically Blunt and Sharp Bodies," *Journal of Spacecraft and Rockets*, Vol. 31, No. 3, 1994, pp. 378–382.

[5]Ianovski, L., Sosounov, V., and Shikhman, Y., "The Application of Endothermic Fuels for High Speed Propulsion Systems," *Papers from the Thirteenth International Symposium on Air Breathing Engines*, Vol. 1, edited by F. S. Billig, AIAA, Reston, VA, 1997, pp. 59–69.

[6]Gurijanov, E. P., and Harsha, P. T., "AJAX: New Directions in Hypersonic Technology," AIAA Paper 96-4609, Nov. 1996.

[7]Ashley, H., and Landahl, M., *Aerodynamics of Wings and Bodies*, 1st ed., Addison–Wesley, Reading, MA, 1965, pp. 178–181.

[8]Rasmussen, M., *Hypersonic Flow*, 1st ed., Wiley, New York, 1994, pp. 288–321.

[9]Freeman, N., Cash, R., and Bedder, D., "An Experimental Investigation of Asymptotic Hypersonic Flows," *Journal of Fluid Mechanics*, Vol. 18, 1964, pp. 379–384.

[10]McGrory, W., Slack, D., Applebaum, M., and Walters, R., *GASP Version 3.0*, Aerosoft, Inc., Blacksburg, VA, 1996.

[11]O'Brien, T. F., and Lewis, M. J., "Power Law Leading Edges for Waveriders Designed with Shock Attachment," AIAA Paper 98-0600, Jan. 1998.

[12]O'Brien, T. F., "Analysis of Power Law Shaped Leading Edges for Waveriders Designed with Shock Attachment," M.S. Thesis, Dept. of Aerospace Engineering, Univ. of Maryland, College Park, MD, Aug. 1998.

[13]Billig, F. S., "Shock-Wave Shapes Around Spherical- and Cylindrical-Nosed Bodies," *Journal of Spacecraft and Rockets*, Vol. 4, No. 6, 1967, pp. 822, 823.

[14]Fay, J. A., and Riddell, F. R., "Theory of Stagnation Point Heat Transfer in Dissociated Air," *Journal of the Aeronautical Sciences*, Vol. 25, No. 2, 1958, pp. 73–85, 121.

[15]White, F. M., *Viscous Fluid Flow*, 1st ed., McGraw–Hill, New York, 1974, pp. 596–600.

J. R. Maus
Associate Editor